





## Research Article

# Micro- and Nanostructure of Layered Si/Sn/Si Films, Formed by Vapor Deposition

V. B. Neimash <sup>1</sup>, P. Ye. Shepelyavyi,<sup>2</sup> A. S. Nikolenko <sup>2</sup>, V. V. Strelchuk <sup>2</sup>  
and V. I. Chegel <sup>2</sup>

<sup>1</sup>*Institute of Physics, National Academy of Sciences of Ukraine, Nauky Ave. 46, Kyiv 03028, Ukraine*

<sup>2</sup>*V.E. Lashkaryov Institute of Semiconductor Physics, National Academy of Sciences of Ukraine, Nauky Ave. 41, Kyiv 03028, Ukraine*

Correspondence should be addressed to V. B. Neimash; [neimash@gmail.com](mailto:neimash@gmail.com)

Received 22 October 2021; Revised 5 April 2022; Accepted 31 May 2022; Published 22 June 2022

Academic Editor: Leander Tapfer

Copyright © 2022 V. B. Neimash et al. This is an open access article distributed under the Creative Commons Attribution License, which permits unrestricted use, distribution, and reproduction in any medium, provided the original work is properly cited.

The peculiarities of surface relief of the Si-Sn-Si layered films, used to produce the silicon nanocrystals with properties of quantum dots, were studied by the methods of electron and atomic force microscopy with the involvement of X-ray fluorescent microanalysis. It was shown that the quasispherical structuring of the relief at the scale 20–20000 nm is typical for the surface of silicon-tin layered films. The role of layer thicknesses is experimentally analyzed under formation of the surface relief (roughness, shapes, and lateral dimensions) during their vacuum deposition from a vapor-gas phase. The peculiarities of the relief of amorphous silicon films deposited on the surface of molten tin are shown. The fractal-like type nanostructuring of amorphous silicon films deposited on the surface of liquid tin was discovered.

## 1. Introduction

Nanocrystalline silicon is considered a promising material for solar cells (CE). It is known that silicon crystals with size order of nanometers acquire the properties of quantum dots [1]. That is, their mechanism of light absorption acquires a quasi-straight-band character, whereas the width of the band gap becomes dependent on the size of the nanocrystal. The use of such nanosilicon to create isomorphous heterostructures of the cascade type [2, 3] can fundamentally increase the efficiency and reduce the cost of SE due to the advantages of thin film and roll technologies [4, 5]. Among the main problems hindering the practical implementation of the advantages of nanosilicon is the insufficient development of technologies for controlling the size and concentration of Si nanocrystals at economically justified film formation rates. Therefore, despite the large number of existing technologies for the production of film nanosilicon (for example, [6–12]), it is important to improve them and search for new ones. One of the promising ways in this direction is the use of the phenomenon of metal-induced crystallization (MIC)

of amorphous silicon [13–17]. The formation of Si nanocrystals with sizes of 2–5 nm and phase volume fraction up to 70% in the amorphous Si matrix by low-temperature tin-induced crystallization of amorphous Si was successfully demonstrated [18–20]. These and other experimental results are well explained by the new MIC mechanism proposed in [20, 21] and theoretically substantiated in [22]. It differs significantly from those known for other metals [13, 15–17]. According to this mechanism, silicon nanocrystals are formed due to the cyclic repetition of the processes of formation and decomposition of a supersaturated solution of silicon in tin in a narrow layer of eutectic at the interface of amorphous silicon and tin metal. It was shown that this mechanism is realized in particular in layered films Si/Sn/Si that reveal the properties of amorphous-crystalline composite, up to 90% of the volume of which is occupied by silicon nanocrystals with a size on the order of nanometers [23]. It was further shown that the MIC of amorphous silicon with the participation of tin can be significantly accelerated by laser irradiation [24–26]. However, a significant obstacle to the practical application of tin-induced crystallization of

amorphous silicon in the manufacture of nanosilicon film is the significant surface roughness such films due to the tendency of tin to form clusters. These significantly prevent the use of MIC in traditional planar technology of silicon instrumentation and therefore require study of its causes and occurrence mechanisms. On the other hand, the same factor provides opportunities for fundamentally new types of micro- and nanostructuring of the surface of silicon films, the properties and prospects of which have not been studied yet. Therefore, the aim of this work was the experimental study of the role of tin in micro- and nanostructuring of the surface of amorphous silicon- tin- amorphous silicon layered films, which are used to create silicon nanocrystals with the properties of quantum dots [12].

## 2. Experiment

The objects of research were 3-layer structures “amorphous silicon-metal tin-amorphous silicon” on the substrates of monocrystalline silicon KEF-4,5. They are made by sequential deposition of silicon (99.999%), tin (99.92%), and again silicon thermally evaporated in vacuum from tantalum evaporators heated by electric current. The deposition took place on polishing up to 6th grade perfection of the monocrystalline silicon substrate of electronic purity with a thickness of  $300\ \mu\text{m}$  at a substrate temperature of  $\sim 150^\circ\text{C}$  in the sequence: a layer of amorphous silicon  $Z$  on a monocrystalline substrate, a layer of tin  $Y$ , and then a second layer of amorphous silicon  $X$  on top of a layer of tin, as shown in Figure 1.

All depositions were carried out in one vacuum chamber without depressurization at a residual pressure of  $10\text{--}3\ \text{Pa}$  by sequential use of 3 different evaporators. The high degree of polishing of the substrate surface guarantees the absence of effects of inhomogeneity of the relief of the base on which the following layers are formed. A lower layer of amorphous silicon  $Z$  with a thickness of 50 or 100 nm is required for better adhesion of the tin layer to the monocrystalline silicon substrate. A layer of tin  $Y$  of different thicknesses in the range of 5-100 nm during next heat treatments functions as a transformer of the silicon phase state from amorphous into nanocrystalline due to MIC effect. Such phase transformation had few influences on the film outer relief that formed at layer deposition. Therefore, it is important to understand the mechanisms of the surface relief during layer deposition before the MIC procedure. In this work, we investigated the forms and quantitative characteristics of the surface microrelief of the layered Si/Sn/Si films at different thickness ratios of silicon and tin layers, as well as the spatial distribution of elemental composition by film area and cross section. To do this, we used an electron microscope JEM-2000FXII on SEM (secondary electron microscopy, equipped with an X-ray dispersion spectrometer AN10000/95S and LZ5 detector with UTW-window), raster electron microscope VEGA 3 SBU, and atomic force microscope NanoScope IIIa Dimension 3000 (Infrared Fourier spectrometer Bruker Vertex 70v). During SEM imaging, two types of detectors were used: BSE, a scattered electron detector at an angle of about 60 degrees to the direction of the electron beam, and detector InBeam, a ring

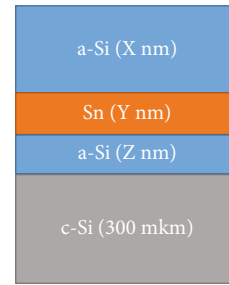


FIGURE 1: Scheme of silicon and tin layers in the studied structures.

detector around the scanning beam that detects mostly electrons reflected at small angles to the beam.

## 3. Results and Discussion

Figure 2 shows SEM images of the surface of the layers of tin (Figure 2(a)), and deposited on it is a layer of amorphous silicon (Figure 2(b)) on a substrate of monocrystalline silicon. The deposition of both layers was performed on a substrate at room temperature.

Figure 2(a) shows that the tin film has a rough relief, despite the mirror surface of the silicon substrate. The shape of its elements is similar to tin crystallites, although the film thickness is much smaller than the literal size of tin crystallites. The silicon film deposited on top of the same thickness (Figure 2(b)) only repeats the relief of the tin film, slightly reducing the roughness. This is an important point to properly understand the results that will be presented below.

The adhesion of tin to the single-crystal silicon substrate is so weak that its layer is easily erased by a finger. Better adhesion can be achieved by depositing tin on a layer of amorphous silicon with a thickness of approximately 50 nm at a substrate temperature of about  $150^\circ\text{C}$ . This is how the  $Z$  layer formed in the studied structures. Its surface has a mirror-smooth surface as well as the surface of the substrate.

During formation of the layer of amorphous silicon  $Y$  by deposition from the gas phase on the heated tin film, it can be melted by the flow of hot Si atoms and heat radiation from the evaporator. In the melted state, thin films of tin  $Y$  under the action of surface tension forces rapidly decompose into microscopic droplets. The main deposition of silicon vapors occurs already on the surface of such melted microdroplets. Accordingly, the shapes and scales of the surface structuring of the amorphous silicon layer  $X$  are determined by the rules of amorphous Si formation on tin melted surface and by the ratio of tin and silicon layer thicknesses.

Figure 3 shows examples of the view in the scanning electron microscope of the surface of the layered structures a-Si/Sn/a-Si, formed in this way. In particular, the surface in Figure 3(d) is very similar to the sample surface in [20, 23]. The Raman spectra of the surface of all these samples correspond to purely amorphous silicon.

It is seen that the shape of the surface structuring of the a-Si layer can vary from spherical to elliptical or irregular convex 4-, 5-, or 6-sided polygon depending on the thickness of the tin layer. In particular, the reduction of Sn thickness

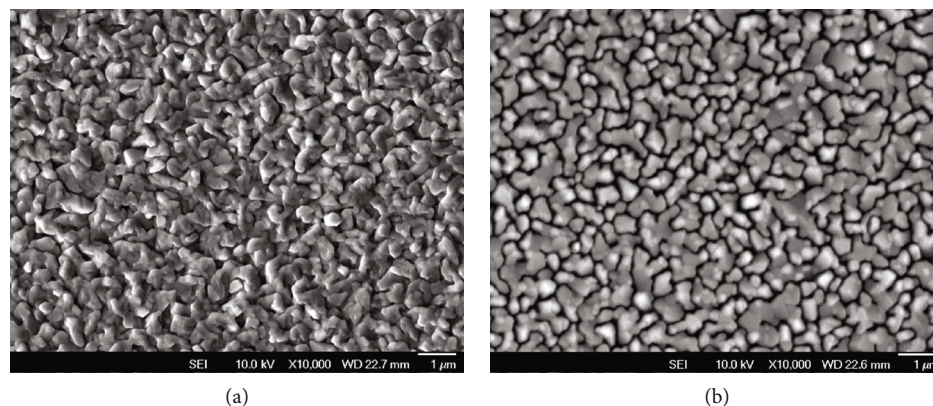


FIGURE 2: SEM imaging of the surface of films deposited from the vapor-gas phase in vacuum on a polished substrate of monocrystalline Si at room temperature: (a) tin; (b) amorphous silicon deposited on top of the tin film. Every layer thickness—100 nm.

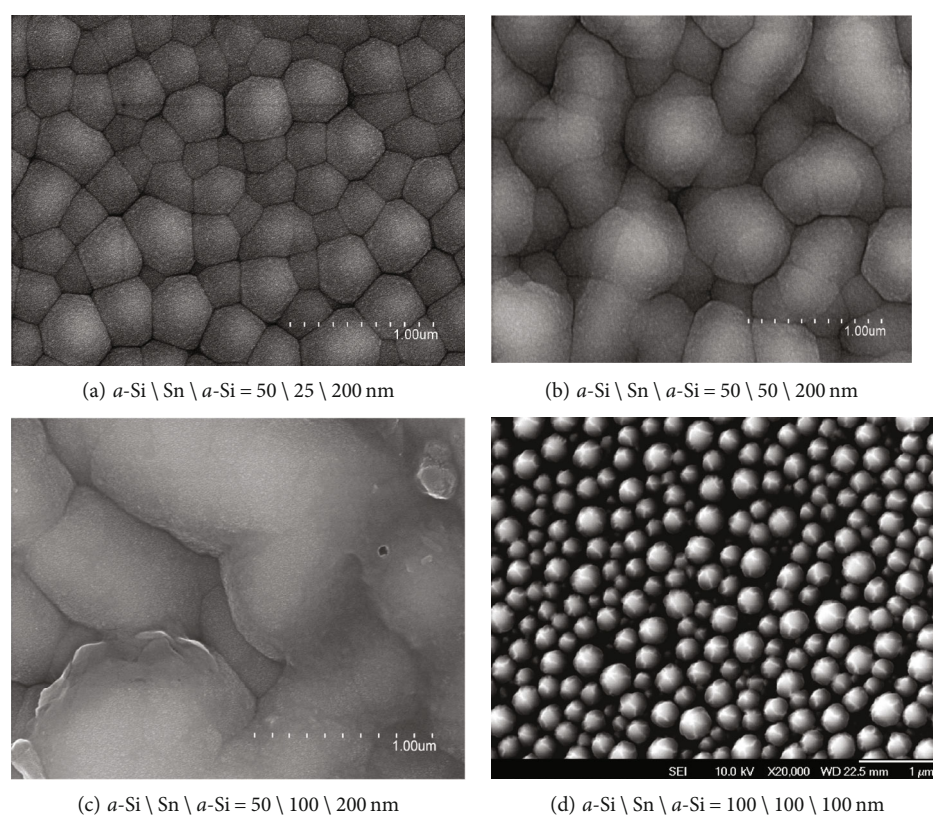


FIGURE 3: SEM image of the surface of layered structures  $a\text{-Si}/\text{Sn}/a\text{-Si}$  with different ratios of layer thickness.

from 100 nm to 25 nm leads to a clearer structuring of the surface, which in shape resembles the structure of soap suds (Figure 3(a)). The scale of surface structuring is also determined by the thickness of the tin layer in such structures. The lateral size of the surface formations is in the range of 200–1000 nm. Figure 4 shows the SEM image of the chipped end of the 3-layer structure  $a\text{-Si}/\text{Sn}/a\text{-Si} = 100/100/200$  nm. A similar cross-sectional view of the 3-layer structure  $a\text{-Si}/\text{Sn}/a\text{-Si}$  has been observed in [27].

Four zones of the contrast level are visible. The first from the bottom is a dark homogeneous zone corresponding to the monocrystalline silicon substrate. Above it,

through the thin light interval, a second dark zone of the lower layer of amorphous silicon Z with a thickness of about 100 nm is observed. Above, layer Y of light hemispheres corresponding to tin drops is clearly visible. This is evidenced by the results of X-ray fluorescence microanalysis, shown in Figure 5.

The high concentration of carbon here is due to carbon contamination of the vacuum chamber of the microscope. This is evidenced by the equality of the C content in spectra 2 of the precipitated film and the substrate of monocrystalline silicon  $\text{изыск}$  3, where the real C content is very low and according to IR analysis does not exceed  $5.10^{16} \text{ cm}^{-3}$ .

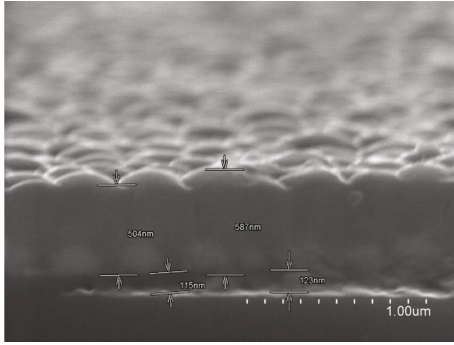
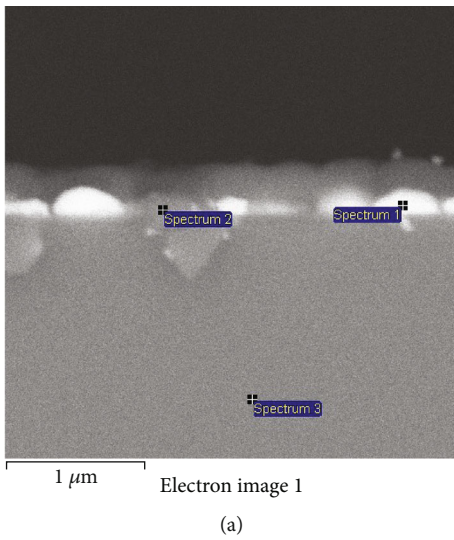


FIGURE 4: SEM cross-sectional image of the 3-layer structure a-Si \ Sn \ a-Si = 100 \ 100 \ 200 nm.



| Spectrum   | C     | O    | Si    | Sn    | Total  |
|------------|-------|------|-------|-------|--------|
| Spectrum 1 | 22.95 | 6.96 | 34.67 | 35.42 | 100.00 |
| Spectrum 2 | 29.72 | 5.00 | 55.19 | 10.09 | 100.00 |
| Spectrum 3 | 29.59 |      | 70.41 |       | 100.00 |

All results in weight %

(b)

FIGURE 5: SEM image of the butt of the layered structure Si \ Sn \ Si. The location of the X-ray microprobe spectrum (a) and the results of the analysis of the elemental composition (b).

The deposition of the outer layer of amorphous silicon X occurs on the drop of tin. Therefore, the surface relief of this silicon layer also has a quasihemispherical shape. As can be seen from Figures 3–5, the thickness of the tin layer Y plays a key role in structuring the relief of the outer surface of the structures a-Si \ Sn \ a-Si both in shape and scale.

To study in more detail the effect of the Y layer of tin on the surface structuring of the amorphous silicon X layer, we used the possibilities of atomic force microscopy. The surface of three layered structures was studied, and their cross-sectional diagram is shown in Figure 6.

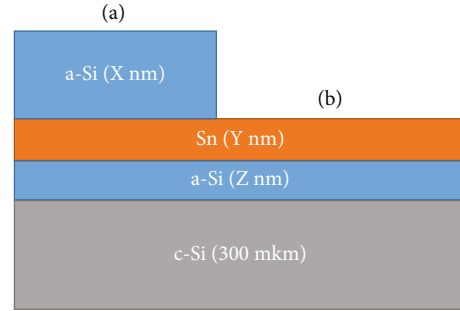


FIGURE 6: The cross-sectional diagram of the studied samples: (a) no. 1—X = 200 nm; Y = 5 nm; Z = 50 nm; (b) no. 1—X = 0; Y = 5 nm; Z = 50 nm; (a) no. 2—X = 200 nm; Y = 10 nm; Z = 50 nm. (b) no. 2—X = 0; Y = 10 nm; Z = 50 nm; (a) no. 3—X = 200 nm; Y = 15 nm; Z = 50 nm; (b) no. 3—X = 0; Y = 15 nm; Z = 50 nm.

It can be seen that each sample consists of two parts: 3-layer part “a” and a 2-layer part “b”, deposited on one substrate under the same conditions. The samples differ only in the thickness of the tin layer Y = 5, 10, and 15 nm. Comparative studies of both parts (Figures 6(a) and 6(b)) of these three samples were performed by atomic force microscopy.

Figures 7–10, for example, show the results of AFM studies of sample no. 3 in pairs of both its parts, i.e., the surfaces of tin and amorphous silicon. The appearance of similar quasispherical formations on the surface of layered structures has been observed under the influence of laser irradiation in [24].

It is seen that quasispherical formations on the surface of the tin layer arose already in the process of its deposition (Figure 7(a)). Their diameter is 250–350 nm, and the range of heights above the surface is 3.7–26.7 nm, i.e., an order of magnitude smaller than the diameter. This is consistent with the above SEM data. Deposition on such a surface of a layer of amorphous silicon with a thickness of 200 nm leads to a significant increase in the diameter of quasispherical formations on the surface while reducing the difference in their heights to the range of 1.4–19.0 nm (Figure 7(b)). Accordingly, there is a decrease in roughness by 1.5–2.0 times, as illustrated in Figure 8. Schematically shown here is the distribution of the height of the relief from its lowest level on the area of  $2 \times 2 \mu\text{m}$  of the surface of the layer of tin (Figure 8(a)) and the silicon (Figure 8(b)) deposited on it.

It should be noted that the ordinate “z” in Figure 8, which corresponds to the height of the deviation of the relief from the minimum level, has a scale 2 orders of magnitude smaller than the ordinates of the surface area “x” and “y.” Therefore, the surface patterns in Figure 8 are not similar to those of previous SEM images, where the scale of all ordinates is the same. However, such presentation of the results of measurements of quantitative parameters of the relief makes it possible to visualize the changes in its roughness due to the deposition of silicon on a layer of tin. For an example of quantitative comparison, Figure 8 shows graphs of one-dimensional surface roughness distribution of the layered structure a-Si (~50 nm)/Sn (~15 nm)/a-Si (~200 nm) before and after deposition of the outer layer of amorphous silicon.

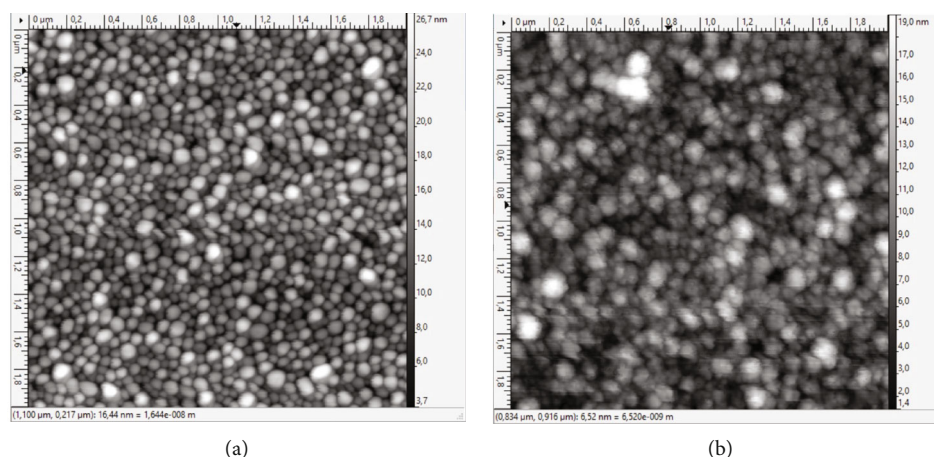


FIGURE 7: AFM image of the surface of layered structures: (a) a-Si (~50 nm)/Sn (~15 nm)-tin outside and (b) a-Si (~50 nm)/Sn (~5 nm)/a-Si (~200 nm)-outwardly amorphous silicon on a common substrate of single-crystal Si.

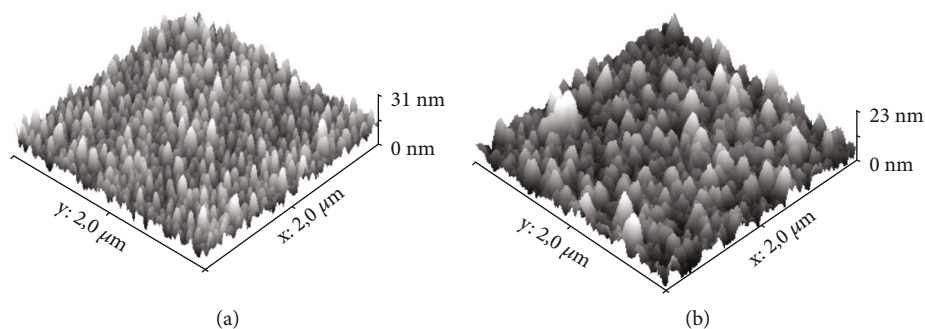


FIGURE 8: Distribution of the height of the relief from its lowest level on the area of  $2 \times 2 \mu\text{m}$  of the surface of the layer of tin (a) and the silicon (b) deposited on it.

The graphs in Figure 9 are reduced to a common denominator in amplitude due to scaling. It is seen that the alignment of the deviation amplitudes is achieved at a scale difference of one and a half times (20 and 30 nm). The average surface roughness after deposition of the silicon layer on the tin layer is reduced by almost half from 13.4 nm to 7.7 nm. As can be seen from Figure 7, the lateral size of quasispherical formations on the surface on the contrary increases after deposition of a 200 nm layer of silicon. Quantitative assessment of this increase by the method of radius of the equivalent disk is presented in Figure 10.

Similar AFM studies were performed on samples of structures with a tin layer thickness of 5 nm and 10 nm. Analysis of the result totality shows the following:

- (i) The formation of drops of tin occurs at the stage of its deposition on silicon heated to  $150^\circ\text{C}$
- (ii) Tin drops have the shape of quasihemispheres with a flat side to the deposition surface (inner layer of amorphous silicon). Their radius, as in the case of thicker layers, correlates with the layer thickness of the deposited tin
- (iii) With the increasing calculated thickness of the tin layer from 5 to 15 nm, the average value of the surface roughness of the tin varies between 3.5 and 19.9 nm, and that of the surface of the outer layer

of silicon above it is 4.2-7.7 nm. The average lateral grain size of the surface increases from 20 to 35 nm and from 15 to 25, respectively

In all three samples, the deposition of the layer of silicon X leads to a decrease in roughness and an increase in grain size. That is, there is a “smoothing” of the surface relief due to the deposition of a much thicker layer of silicon. Nevertheless, a certain part of the tin appears on the surface again. This is illustrated in Figure 11.

You can see some almost perfectly spherical drops of tin with a diameter up to  $2 \mu\text{m}$ , which lie on the surface of amorphous silicon X (Figures 11(a) and 11(b)) and are free from silicon coating. There are much smaller (0.2-0.4  $\mu\text{m}$ ) drops partially covered with silicon (Figures 11(b)–11(d)). But most tin drops of 100-300 nm scale are covered with a layer of silicon, forming a solid surface (Figures 3–5).

Figure 12 shows the results of X-ray fluorescence microanalysis of these objects. They show that blonde spheres on the surface and blonde parts of the hemispheres in the surface consist mainly of tin. Dark spheres on the surface and dark hemispheres in the surface contain mainly silicon.

A comparison of Figures 11(c) and 11(d) illustrates the difference in magnification and SEM resolution when using BSE and InBeam detectors. The transition to the “InBeam” mode allows us to notice that the quasispherical formations

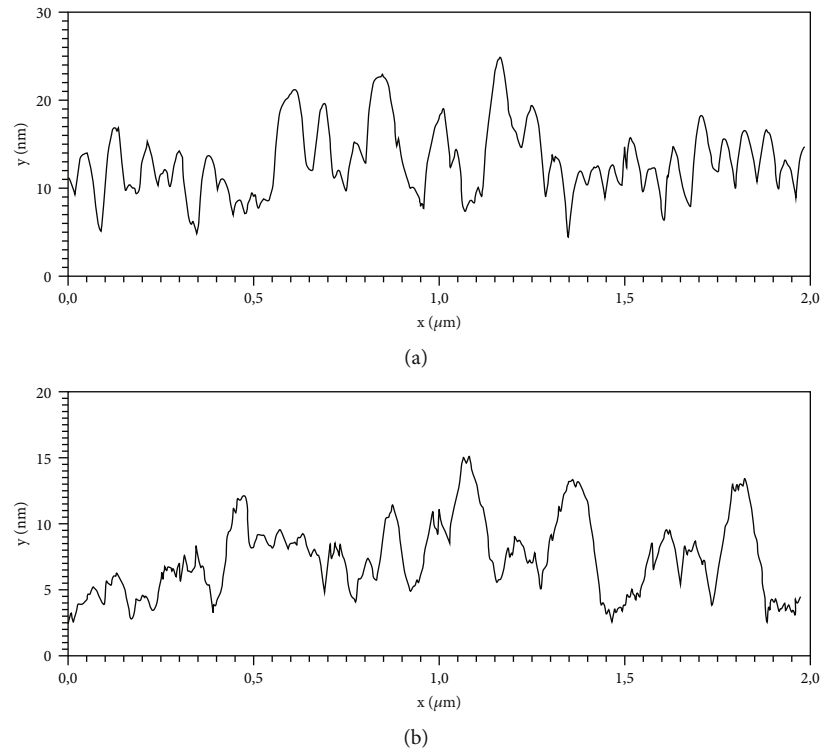


FIGURE 9: One-dimensional distribution of surface roughness of structures a-Si (~50 nm)/Sn (~15 nm)/a-Si (~200 nm) (a) and a-Si (~50 nm)/Sn (~15 nm)/a-Si (~200 nm) (b).

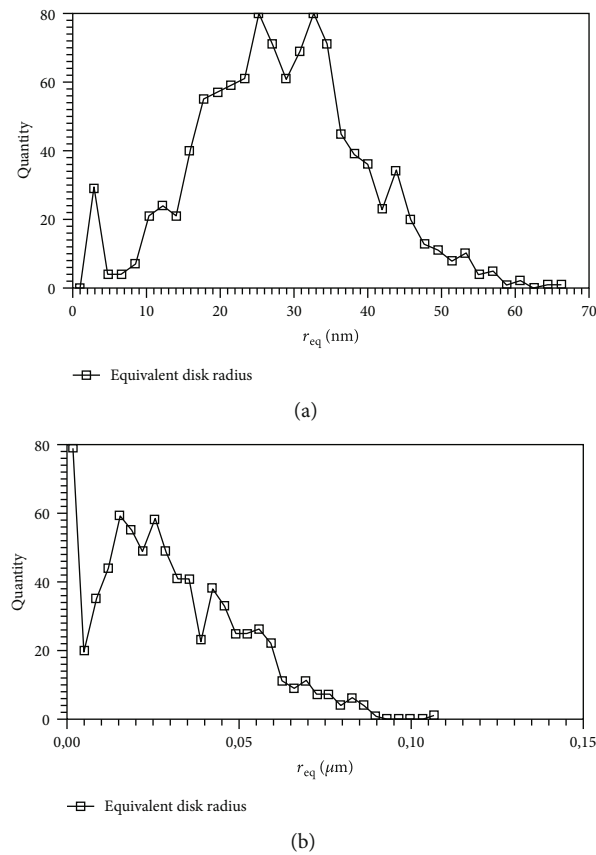


FIGURE 10: Size distribution of quasispherical formations on the surface of layers of tin and silicon structures: (a) a-Si (~50 nm)/Sn (~15 nm) and (b) a-Si (~50 nm)/Sn (~15 nm)/a-Si (~200 nm) in the approximation of the equivalent disk radius.

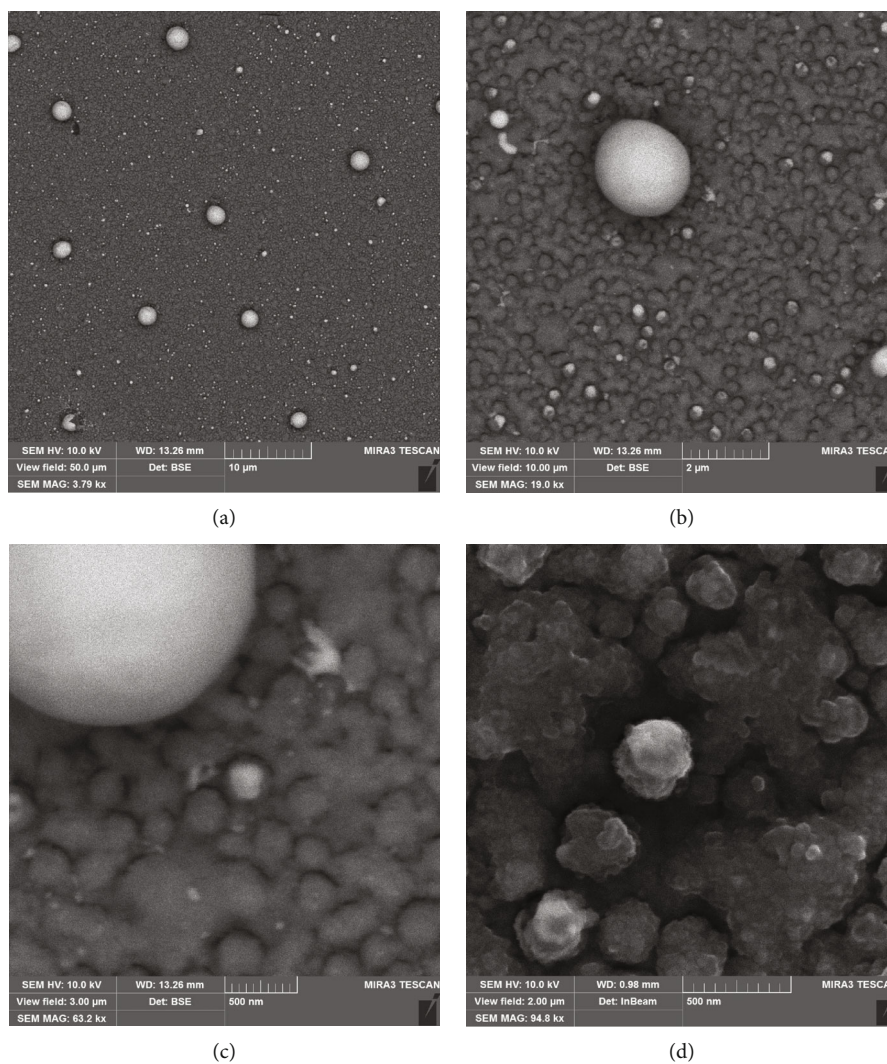
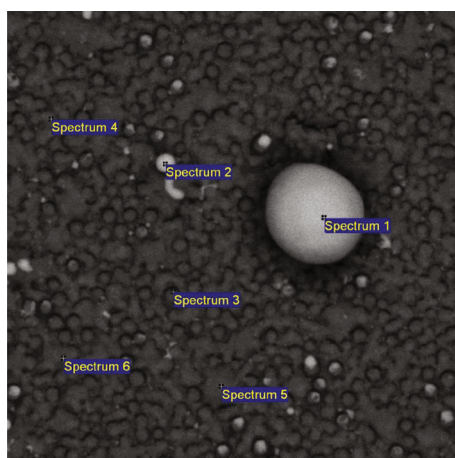


FIGURE 11: SEM images of a-Si (~50 nm)/Sn (~15 nm)/a-Si (~200 nm) structure surface at different magnifications (a–c) and detectors (c, d).



| Spectrum   | In stats. | C     | N    | O     | Si    | Sn    | Total  |
|------------|-----------|-------|------|-------|-------|-------|--------|
| Spectrum 1 | Yes       | 2.95  | 1.41 | 5.85  | 1.42  | 88.36 | 100.00 |
| Spectrum 2 | Yes       | 3.49  | 1.56 | 6.46  | 9.93  | 78.55 | 100.00 |
| Spectrum 3 | Yes       | 9.88  |      | 9.89  | 63.99 | 16.24 | 100.00 |
| Spectrum 4 | Yes       | 10.26 | 0.00 | 10.18 | 63.12 | 16.44 | 100.00 |
| Spectrum 5 | Yes       | 10.98 |      | 8.13  | 64.97 | 15.92 | 100.00 |
| Spectrum 6 | Yes       | 8.15  |      | 7.89  | 71.06 | 12.90 | 100.00 |

All results in weight %

(a)

(b)

FIGURE 12: Spatial (a) and concentration (b) distributions of the main chemical elements over the surface layer of the sample a-Si (~50 nm)/Sn (~15 nm)/a-Si (~200 nm).

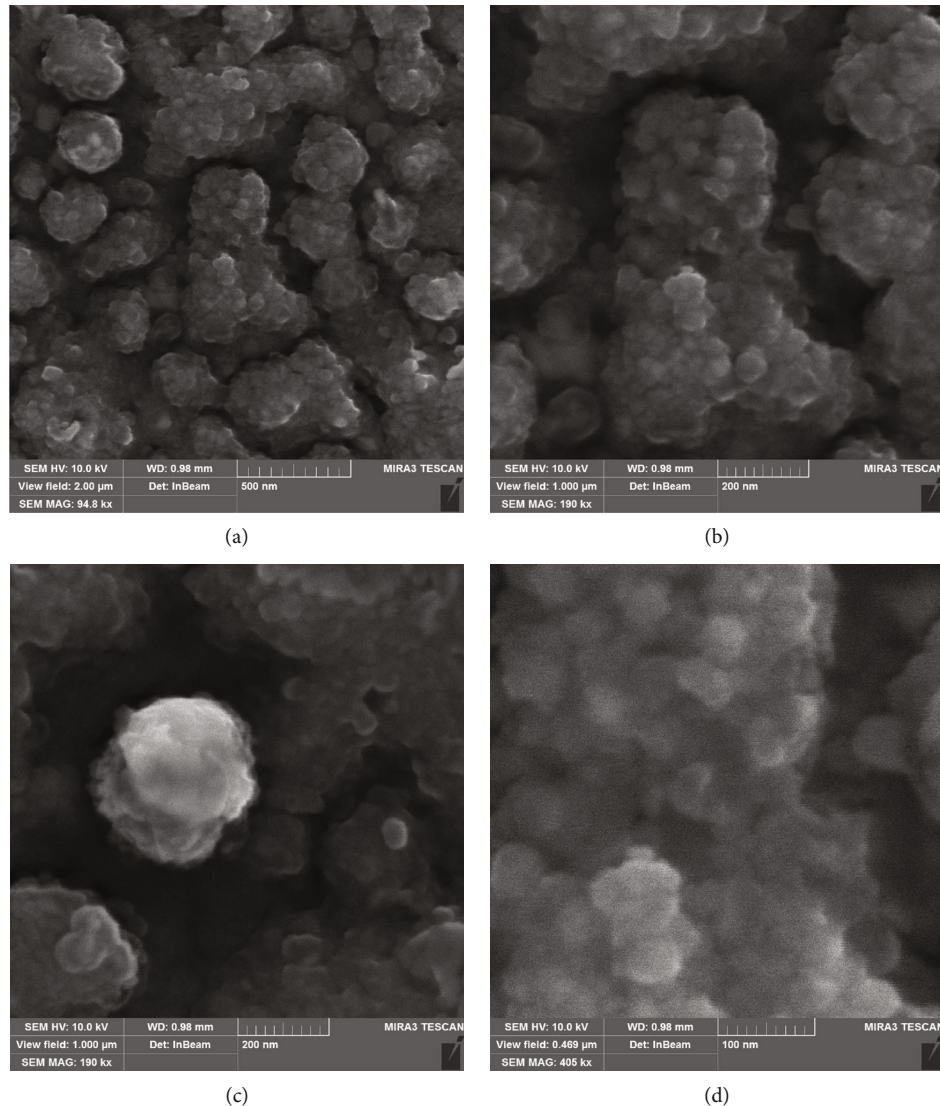


FIGURE 13: SEM images due to “InBeam” detectors of the a-Si (~50 nm)/Sn (~15 nm)/a-Si (~200 nm) structure surface at different magnifications.

on the surface of samples have a more complex structure. At higher magnification, it becomes obvious that they consist of smaller (of an order of magnitude) quasispherical formations.

This is clearly seen in Figure 13. The smallest formations, which are clearly separated here, have a size of less than 20 nm. They form structures similar to 3-dimensional dendrites or grapes.

These results are in good agreement with the AFM data on roughness and grain size (Figures 7–10).

In our opinion, the experimental results presented here allow us to draw the following conclusions.

#### 4. Conclusions

- (1) The primary structuring of Si/Sn/Si layered films occurs during the deposition of the Y-layer in the form of hemispherical microdroplets of tin on a flat Z-layer of amorphous silicon. The reasons for this are the temperature of the Z-layer above the melting

point of Sn, low adhesion of Sn to Si, and the surface tension of liquid Sn. Hemispherical tin droplets have a literal size and thickness of tens to hundreds of nanometers, depending on the thickness of the Y-layer, i.e., the amount of deposited tin

- (2) X-layer relief of the amorphous silicon deposited on the Y-layer of tin in general repeats the quasispherical structure of the relief of the Y-layer. Thickness increase in the X-layer leads to a decrease in the relief roughness and increase in the literal size of quasispherical formations. The ratio of the X- and Y-layer thicknesses also affects the shape, literal size, and roughness of the formations. The use of these dependences allows one to adjust the light-reflecting properties of such films from mirror to soot-like
- (3) Secondary structuring occurs as a result melting of tin hemispheres in the Y-layer during deposition the outer silicon X-layer. The flow of hot silicon



vapors and radiation from evaporator melt the tin in the Y-layer. Therefore, silicon X-layer deposition occurs on the molten metal surface. Low solubility of silicon in tin at near-melting temperatures and poor adhesion between Sn and Si, in our opinion, leads to the formation of the amorphous silicon X-layer in the form of fractal dendrites and the corresponding structuring of its surface in scale of tens nanometers

- (4) Tin segregation at the growing solid (amorphous) phase front of silicon together with surface tension forces can promote the formation of a new generation of tin droplets and their penetration on X-layer surface through pores between dendrites of amorphous silicon. Presumably, the dynamic nature of these processes leaves room for the existence of both small (20–200 nm) tin droplets, covered with a layer of silicon and large (1–2  $\mu\text{m}$ ) single tin droplets on the surface without any traces of silicon deposition on them
- (5) The results obtained in this work can be used to improve existing technologies for the formation of film nanosilicon by tin-induced crystallization of amorphous silicon, as well as for the manufacture of light-scattering coatings

## Data Availability

The data used to support the findings of this study are available from the Institute of Physics of National Academy of Science of Ukraine upon request on Report on the results of the 1st stage of the research project number 12\20-H “Tin-induced volume nanocrystallization and surface nanostructuring of amorphous silicon thin films”.

## Conflicts of Interest

The authors declare that they have no conflicts of interest.

## Acknowledgments

The work was supported by the Target Comprehensive Program of the National Academy of Sciences of Ukraine “Fundamental problems of creating new nanomaterials and nanotechnologies” within the competition project no. 12\20-H “Tin-induced volume nanocrystallization and surface nanostructuring of amorphous silicon thin films”.

## References

- [1] M. C. Beard, J. M. Luther, and A. J. Nozik, “The promise and challenge of nanostructured solar cells,” *Nature nanotechnology*, vol. 9, no. 12, pp. 951–954, 2014.
- [2] Z. I. Alferov, V. M. Andreev, and V. D. Rumyantsev, “Solar photovoltaics: trends and prospects,” *Semiconductors*, vol. 38, no. 8, pp. 899–908, 2004.
- [3] B. Yan, G. Yue, X. Xu, J. Yang, and S. Guha, “High efficiency amorphous and nanocrystalline silicon solar cells,” *Physica Status Solidi*, vol. 207, no. 3, pp. 671–677, 2010.
- [4] N. S. Lewis, “Toward cost-effective solar energy use,” *Science*, vol. 315, no. 5813, pp. 798–801, 2007.
- [5] R. Søndergaard, M. Hösel, D. Angmo, T. T. Larsen-Olsen, and F. C. Krebs, “Roll-to-roll fabrication of polymer solar cells,” *Materials Today*, vol. 15, no. 36, 2012.
- [6] M. Birkholz, B. Selle, E. Conrad, K. Lips, and W. Fuhs, “Evolution of structure in thin microcrystalline silicon films grown by electron-cyclotron resonance chemical vapor deposition,” *Journal of Applied Physics*, vol. 88, no. 7, p. 4376, 2000.
- [7] B. Rech, T. Roschek, J. Müller, S. Wieder, and H. Wagner, “Amorphous and microcrystalline silicon solar cells prepared at high deposition rates using RF (13.56 MHz) plasma excitation frequencies,” *Solar Energy Materials and Solar Cells*, vol. 66, p. 267, 2001.
- [8] Y. Mai, S. Klein, R. Carius et al., “Improvement of open circuit voltage in microcrystalline silicon solar cells using hot wire buffer layers,” *Journal of Non-Crystalline Solids*, vol. 352, p. 1859, 2006.
- [9] H. Li, R. H. Franken, R. L. Stolk, C. H. M. van der Werf, J. K. Rath, and R. E. I. Schropp, “Controlling the quality of nanocrystalline silicon made by hot-wire chemical vapor deposition by using a reverse H<sub>2</sub> profiling technique,” *Journal of Non-Crystalline Solids*, vol. 354, p. 2087, 2008.
- [10] R. Amrani, F. Pichot, L. Chahed, and Y. Cuminal, “Amorphous-nanocrystalline transition in silicon thin films obtained by argon diluted silane PECVD,” *Crystal Structure Theory and Applications*, vol. 1, no. 3, pp. 57–61, 2012.
- [11] G. Fugallo and A. Mattoni, “Thermally induced recrystallization of textured hydrogenated nanocrystalline silicon,” *Physical Review B*, vol. 89, p. 045301, 2014.
- [12] S. Morozova, V. Alikina, F. Vinogradov, and M. Pagliaro, “Silicon quantum dots: synthesis, encapsulation, and application in light-emitting diodes,” *Frontiers in Chemistry*, vol. 8, 2020.
- [13] O. Nast and A. J. Hartmann, “Influence of interface and Al structure on layer exchange during aluminum-induced crystallization of amorphous silicon,” *Journal of Applied Physics*, vol. 88, no. 2, pp. 716–724, 2000.
- [14] Metal-induced crystallization, *Fundamentals and Applications*, Z. Wang, L. P. H. Jeurgens, and E. J. Mittemeijer, Eds., Pan Stanford Publishing, 2014.
- [15] K. Toko and T. Suemasu, “Metal-induced layer exchange of group IV materials,” *Journal of Physics D: Applied Physics*, vol. 53, p. 373002, 2020.
- [16] D. Van Gestel, I. Gordon, and J. Poortmans, “Aluminum-induced crystallization for thin-film polycrystalline silicon solar cells: achievements and perspective,” *Solar Energy Materials and Solar Cells*, vol. 119, p. 261, 2013.
- [17] A. Mohiddon and G. Krishna, “Metal induced crystallization,” in *Crystallization—Science and Technology*, A. Marcelllo, Ed., p. 461, InTech, 2012.
- [18] V. V. Voitovych, V. B. Neimash, N. N. Krasko et al., “The effect of Sn impurity on the optical and structural properties of thin silicon films,” *Semiconductors*, vol. 45, p. 1281, 2011.
- [19] V. B. Neimash, V. M. Poroshin, A. M. Kabaldin et al., “Microstructure of thin Si–Sn composite films,” *Ukrainian Journal of Physics*, vol. 58, no. 9, pp. 865–871, 2013.
- [20] V. Neimash, V. Poroshin, P. Shepeliavii et al., “Tin induced a-Si crystallization in thin films of Si–Sn alloys,” *Journal of Applied Physics*, vol. 114, p. 213104, 2013.
- [21] V. B. Neimash, A. O. Goushcha, P. E. Shepeliavii et al., “Mechanism of tin-induced crystallization in amorphous silicon,”

- Ukrainian Journal of Physics*, vol. 59, no. 12, pp. 1168–1176, 2014.
- [22] V. B. Neimash, A. O. Goushcha, P. Y. Shepeliavyi, V. O. Yuhymchuk, V. V. Melnyk, and A. G. Kuzmich, “Self-sustained cyclic tin induced crystallization of amorphous silicon,” *Journal of Materials Research*, vol. 30, no. 20, p. 3116, 2015.
- [23] V. Neimash, P. Shepelyavyi, G. Dovbeshko et al., “Nanocrystals Growth Control during Laser Annealing of Sn:( $\alpha$ -Si) Composites,” *Journal of Nanomaterials*, vol. 2016, Article ID 7920238, 8 pages, 2016.
- [24] V. B. Neimash, A. O. Goushcha, L. L. Fedorenko et al., “Role of Laser Power, Wavelength, and Pulse Duration in Laser Assisted Tin- Induced Crystallization of Amorphous Silicon,” *Journal of Nanomaterials*, vol. 2018, Article ID 1243685, 11 pages, 2018.
- [25] V. B. Neimash, A. S. Nikolenko, V. V. Strelchuk et al., “Formation of nanocrystals and their properties during tin induced and laser light stimulated crystallization of amorphous silicon,” *Semiconductor Physics, Quantum Electronics & Optoelectronics*, vol. 22, no. 2, pp. 206–214, 2019.
- [26] V. B. Neimash, A. S. Nikolenko, V. V. Strelchuk et al., “Influence of laser light on the formation and properties of silicon nanocrystals in a-Si/Sn layered structures,” *Ukrainian Journal of Physics*, vol. 64, no. 6, p. 522, 2019.
- [27] V. Neimash, “Physical vapor deposition for tin-induced and laser crystallization,” in *Chapt. 15 in nanostructured semiconductors: amorphization and thermal properties*, K. Termentzidis, Ed., pp. 391–424, Pan Stanford Publishing Pte. Ltd, 2017.